Development of Higher-Order Accurate Computational Fluid Dynamic Method for Steam Flow Analysis in Steam Turbines

Xin Yuan[1*], Zhirong Lin[1] and Tadashi Tanuma[2]

[1] Department of Thermal Engineering, Tsinghua University, Beijing 100084, P. R. China
[*]E-mail: yuanxin@tsinghua.edu.cn
[2] Toshiba Corporation, Yokohama 230-0045, Japan

A higher-order robust computational fluid dynamic method has been proposed to wet steam flow analysis in steam turbines. The Favre-averaged compressible Navier-Stokes equations are chosen as governing equations, a general equation of state is used for real fluid instead of perfect gas. The steam/water properties and their derivatives are obtained from IAPWS-IF97 formula. A four-equation model of non-equilibrium steam-droplet spontaneous condensing flows is solved simultaneously with Navier-Stakes equations using an implicit LU-SGS-GE scheme and a modified fourth-order MUSCLE TVD scheme; those have been extended for the real fluid. A code using the above method has been developed; and numerical results of three cases in a three-dimensional last-stage steam turbine nozzle are predicted and partly verified with measured data.

1. Introduction

The steam turbine is one of the most important core machineries in power system. In order to further increase its efficiency, we have to know the mechanism of steam flow from dry steam to wet steam at design/off-design conditions within the steam turbine as clearly as possible.

In past some decades, the application of computational fluid dynamics (CFD) in the turbomachinery has been carried out by many researchers, but these simulations are often for perfect gas flow. For steam condensing flow, the accuracy depends ultimately on the theories of nucleation and droplet growth. For nucleation theories, the classical theory with non-isothermal effects correction agrees with the experimental data precisely. For droplet growth theories, the situation is more complicated. A number of different equations have been derived by different authors, which give widely differing results. The references [1, 2] attempted to derive a general equation with a wide scope of application.

With the above relevant mathematical models, some works about condensing flows simulation have been done by using several-equation models (e.g. a two- or four-equation model) [3-5].

In previous study, we proposed a higher-order robust CFD method for the perfect gas flow [6, 7], and applied it to design and develop the turbine blades successfully [8]. In the present paper, we develop this method to the non-equilibrium wet steam flow. The numerical results including the single phase flow; the equilibrium two phase flows and the non-equilibrium two phase flows in the last-stage steam turbine nozzle are predicted and partly verified with measured data [9].

2. Governing Equations

The basic equations governing spontaneous gas-liquid two-phase fluid condensing flows in steam turbines are the Favre-averaged compressible Navier-Stokes equations, which are based on the laws of conservation of mixture mass, momentum and energy. These equations may be written in a Cartesian coordinate system as

$$\frac{\partial \rho}{\partial t} + \frac{\partial}{\partial x_i}(\rho u_i) = 0 \tag{1}$$

$$\frac{\partial}{\partial t}(\rho u_l) + \frac{\partial}{\partial x_i}(\rho u_l u_i + \delta_{il} p) = \frac{\partial \tau_{il}}{\partial x_i} \tag{2}$$

$$\frac{\partial}{\partial t}(\rho E) + \frac{\partial}{\partial x_i}(\rho H u_i) = \frac{\partial}{\partial x_i}(\tau_{ij} u_j - q_i) \tag{3}$$

where t is the time, x_i are the Cartesian coordinate components, ρ is the density, u_i are the x_i components of velocity vector, δ_{ij} is Kronecker delta, $E = e + u_l u_l / 2$ and $H = h + u_l u_l / 2$ are the total specific energy and enthalpy, where e and h

are the specific internal energy and enthalpy respectively. The pressure is represented from the general equation of state for real fluid as

$$p = p(\rho, \rho e) \tag{4}$$

where ρ and ρe are selected as the independent variables because they are taken from the basic conservation equations (1) and (3) directly. τ_{ij} and q_i are the components of the total stress tensor and heat-flux vector, respectively, which include both molecular and turbulent contributions.

In order to solve the turbulence flow, the eddy viscosity μ_t for general two-equation turbulence models is represented in terms of additional field variables here taken to be ϑ_1 and ϑ_2 so that $\mu_t = \mu_t(\vartheta_1, \vartheta_2)$. The additional field equations governing ϑ_1 and ϑ_2 are written as

$$\frac{\partial}{\partial t}(\rho\vartheta_m) + \frac{\partial}{\partial x_i}(\rho\vartheta_m u_i) = \frac{\partial}{\partial x_i}\left[\left(\mu + \frac{\mu_t}{\mathrm{Pr}_{\vartheta_m}}\right)\frac{\partial \vartheta_m}{\partial x_i}\right] + S_{\vartheta_m} \tag{5}$$

where μ is the molecular viscosity, S_{ϑ_m} are the source functions of the two-equation turbulence models. The modeling constants $\mathrm{Pr}_{\vartheta_m}$ are dependent on the turbulence models used. A low-Reynolds-number q-ω two-equation turbulence model is used in the present paper [10].

The non-equilibrium condensation consists of nucleation and growth of the existing droplets. The equations for nucleation and water droplet growth model [3, 4] which are used for the present paper can be written as

$$\frac{\partial}{\partial t}(\rho\beta_n) + \frac{\partial}{\partial x_i}(\rho\beta_n u_i) = S_{\beta_n} \tag{6}$$

where β_1 is the wetness mass fraction, β_2, β_3 and β_4 are the total surface area, total radius, and number density of the droplets per unit mass, S_{β_n} are the source functions of the four-equation model.

In order to solve conveniently, the governing equations are often written as dimensionless form. The conservation laws for the basic flow quantities ρ, ρu_l, ρE, $\rho\vartheta_m$ and $\rho\beta_n$, which are in (1)-(3), (5) and (6), may be written in the non-dimensional compact vector form as

$$\frac{\partial \boldsymbol{Q}}{\partial t} + \frac{\partial \boldsymbol{F}_i}{\partial x_i} + \frac{1}{\mathrm{Re}}\boldsymbol{\Phi} + \boldsymbol{S} = 0 \tag{7}$$

$$\boldsymbol{Q} = \begin{bmatrix} \rho \\ \rho u_1 \\ \rho u_2 \\ \rho u_3 \\ \rho E \\ \rho\vartheta_m \\ \rho\beta_n \end{bmatrix} \quad \boldsymbol{F}_i = \begin{bmatrix} \rho u_i \\ \rho u_1 u_i + \delta_{i1} p \\ \rho u_2 u_i + \delta_{i2} p \\ \rho u_3 u_i + \delta_{i3} p \\ \rho H u_i \\ \rho\vartheta_m u_i \\ \rho\beta_n u_i \end{bmatrix}$$

$$\boldsymbol{\Phi} = -\frac{\partial}{\partial x_i}\begin{bmatrix} 0 \\ \tau_{i1} \\ \tau_{i2} \\ \tau_{i3} \\ \tau_{ij}u_j - q_i \\ \varpi_i(\vartheta_m) \\ 0 \end{bmatrix} \quad \boldsymbol{S} = -\begin{bmatrix} 0 \\ 0 \\ 0 \\ 0 \\ 0 \\ S_{\vartheta_m} \\ S_{\beta_n} \end{bmatrix} \tag{8}$$

$$\tau_{ij} = (\mu + \mu_t)\left(\frac{\partial u_i}{\partial x_j} + \frac{\partial u_j}{\partial x_i} - \frac{2}{3}\delta_{ij}\frac{\partial u_l}{\partial x_l}\right) - \frac{2}{3}\delta_{ij}\rho k\,\mathrm{Re}$$

$$q_i = -\left(\frac{\mu}{\mathrm{Pr}} + \frac{\mu_t}{\mathrm{Pr}_t}\right)\frac{\partial h}{\partial x_i},\ \varpi_i(\vartheta_m) = \left(\mu + \frac{\mu_t}{\mathrm{Pr}_{\vartheta_m}}\right)\frac{\partial \vartheta_m}{\partial x_i}$$

where k is the turbulence kinetic energy, Pr and Pr_t are the laminar and turbulent Prandtl numbers, Re is the Reynolds number, which is composed of characteristic variables.

As the numerical simulation is solved at the geometric region having an arbitrary shape, the governing equations (7) may be written in the general curvilinear coordinate ξ_i system as

$$\frac{\partial \hat{\boldsymbol{Q}}}{\partial t} + \frac{\partial \hat{\boldsymbol{F}}_i}{\partial \xi_i} + \frac{1}{\mathrm{Re}}\hat{\boldsymbol{\Phi}} + \hat{\boldsymbol{S}} = 0 \tag{9}$$

3. Numerical Method

In order to solve the present governing equations simultaneously, we propose an especially combined method, which is a convergence-accelerated, higher-order; high resolution numerical algorithm based on the implicit time-marching finite difference method, and is used for the real fluid. The present method mainly includes LU-SGS-GE implicit scheme [6], the modified fourth-order high resolution MUSCL TVD scheme [7], etc.

3.1. Specification of Linearization for Real Fluid To use the above numerical method, we need to linearize the governing equations. The linearization is performed to the inviscid flux vectors $\boldsymbol{F}_i$ in equation (7), while the Jacobian matrices may be written as $\boldsymbol{A}_i = \partial \boldsymbol{F}_i / \partial \boldsymbol{Q}$. Distinctly, it is necessary to show the pressure p into a function of $\boldsymbol{Q}$. Since, it is difficult to write $p(\boldsymbol{Q})$ for the real fluid directly, we introduced an equation which would be used with the equation of state for real fluid (4) as follows

$$\rho e = \rho E - \frac{1}{2}\frac{(\rho u_l)(\rho u_l)}{\rho} \tag{10}$$

The partial derivative of p with respect to ρ of $\boldsymbol{Q}$ can be deduced as follows:

$$\frac{\partial p}{\partial \rho} = \frac{\partial p}{\partial (\rho e)}\bigg|_{\rho} \frac{\partial (\rho e)}{\partial \rho}\bigg|_{\boldsymbol{Q}\ \text{except}\ \rho} + \frac{\partial p}{\partial \rho}\bigg|_{\rho e} \frac{\partial \rho}{\partial \rho}\bigg|_{\boldsymbol{Q}\ \text{except}\ \rho} \tag{11}$$

If we define two variables $p'_e = \partial p / \partial (\rho e)\big|_{\rho}$ and $e'_{\rho} = \partial (\rho e) / \partial \rho\big|_{p}$, and deduce lengthily, we can get $\partial p / \partial \rho = p'_e (u_l u_l / 2 - e'_{\rho})$. Similarly, we can get other relative parameters too. Where p'_e and e'_{ρ} are determined by using the reconstructed table of real fluid with the piecewise linear interpolation.

3.2. Higher-Order Robust CFD Method A specially combined LU-SGS-GE scheme is extended for solving the present Favre-averaged compressible Navier-Stokes equations, the low-Reynolds-number q-ω two-equation turbulence model, and the non-equilibrium four-equation condensation model simultaneously. Because the similarity transforms are used accurately to construct upstream Jacobian matrices of flux vectors in the implicit LU-SGS-GE scheme, it leads to much faster convergence, better stability without improper numerical dissipation and free-parameters. The most excellence is 11×11 quasi-block-diagonal matrix in the LU-SGS-GE scheme can be simplified into 4×4 sub-matrix, the block-diagonal matrix inversion are still eliminated partly, and the implicit operator can also be vectored completely. A modified fourth-order, high resolution compact MUSCL TVD scheme is implemented to accurately solve the unsteady three-dimensional (3D) real fluid flows. The modified fourth-order MUSCL TVD scheme consists of two-level limiter, which operates on the first- and second-order differences of unknown variables respectively; the improper numerical oscillations due to higher-order extrapolations are avoided.

4. Computation Setup

4.1. Computational Grid A kind of geometric grid generation method is applied to obtain the 3D structure grid. Figure 1 shows the sketch of 3D grid of the last-stage steam turbine nozzle blade, and its typical two-dimensional section along the spanwise of this nozzle blade.

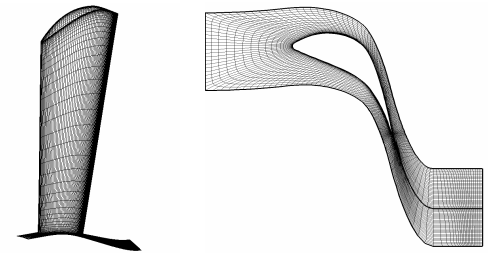

a) 3D grid b) A section of 3D grid

Fig. 1. The sketch of computational grid.

4.2. Models for Flow Medium Three kinds of different models for different flow medium were considered in the present paper.

Case 1 (Perfect Gas Case) is for the model of perfect gas, which means a simple thermophysical formula $p = \rho RT$ is available in this case.

Case 2 (Equilibrium Case) is for the model of equilibrium wet steam. The equilibrium means there are still two independent variables in a closed system, because there is a one-to-one correspondence between temperature T and static pressure p under this situation while a new parameter of wetness β_1 is independent. The conservational parameters ρ and ρe are selected as the two independent variables in the present paper. Then the equilibrium wet steam flow can be treated as a general single phase system, notwithstanding it consists of steam and water phases actually.

Case 3 (Non-equilibrium Case) is for the model of non-equilibrium spontaneous condensing wet steam flow. In this case, β_1 becomes also an independent parameter. In order to obtain the distribution of β_1, a classical four-equation spontaneous condensing model is solved simultaneously with the governing equations.

The property data of steam and water are fully obtained from IAPWS-IF97 [11] in case 2 and 3.

4.3. Boundary Conditions The outlet boundary conditions for the three different cases were the same exactly, but different treatments were applied for the inlet boundary conditions.

For case 1, the conventional inlet boundary conditions including the total pressure p_0 , total temperature T_0 and flow angles are employed.

For case 2, the same inlet state point as case 1 is maintained. Because the steam is already enter saturation area at inlet and very close to saturation point, so T_0 can be educed by p_0 actually. That means p_0 and T_0 can not be set at the same time. Considering this problem, another two parameters, total enthalpy H_0 and entropy s , are used as inlet boundary conditions instead of p_0 and T_0 . In a word, the inlet state point of case 1 and case 2 is identical, but different independent variables are chosen to express the same state point.

For case 3, the inlet boundary conditions are almost the same as case 2. But some additional information must be added to describe the water droplets. These additional boundary conditions include wetness, averaged droplet surface area, averaged droplet radius and total droplet number.

5. Results and Discussions

5.1. Comparisons of Flow Fields The developed CFD method were applied to solve wet steam flows in a low-pressure (LP) last stage stator blade for a typical large-scale steam turbine. The steam flow conditions are provided from aero-thermal measurement data of a model test steam turbine [9]. Inlet wetness fraction is the same as the LP last stage inlet condition of a typical large-scale steam turbine for fossil power plants. Inlet supercooling is defined as zero for the present numerical study.

In the three cases, only case 3 can provide valid information about the degree of supercooling, i.e. the levels of non-equilibrium state. Figure 2 shows the computational result of the case 3, non-equilibrium flow.

The equilibrium state is set at inlet boundary, so the degree of supercooling is zero there. The steam flow kept expanding and cooling along the streamlines, and the degree of supercooling also kept increasing. It reached the max value of about 20 ºC near the trailing-edge area. In the present case, it can be found that the droplet grew very slow and the steam flow couldn't recover to equilibrium state in a short time.

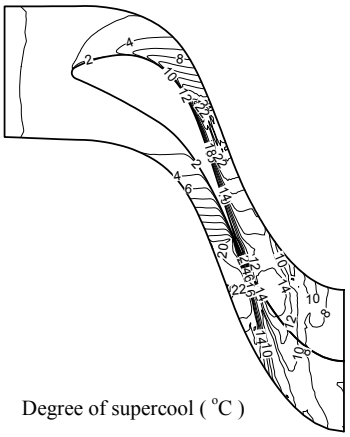

Fig. 2. Distribution of supercooling at 50% span.

Although the model of the wet steam flow is different for the three cases, the flow patterns are still similar due to the same boundary conditions on the blade surfaces. The distributions of relative static pressure for different cases are plotted in Fig. 3. The relative static pressures are local static pressures divided by inlet average total pressure.

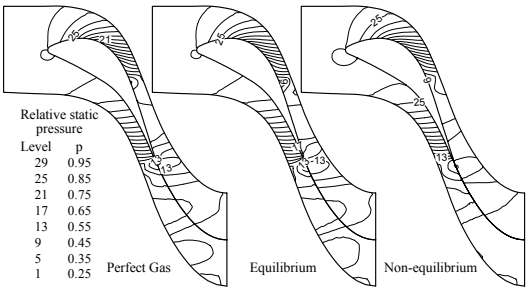

Fig. 3. Relative static pressure distributions at 50% span.

Figure 4 shows the detail of the temperature distributions, it shows much different among the three cases. In case 1 and 3, the temperature changes faster than which in case 2 because the temperature variation is partly substituted by phase transformation in case 2.

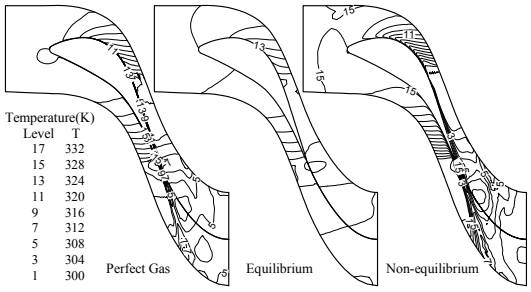

Fig. 4. Temperature distributions at 50% span.

The distributions of Mach number for the three cases are similar too, which also indicate the same flow pattern for different cases. The detail is shown in Fig. 5.

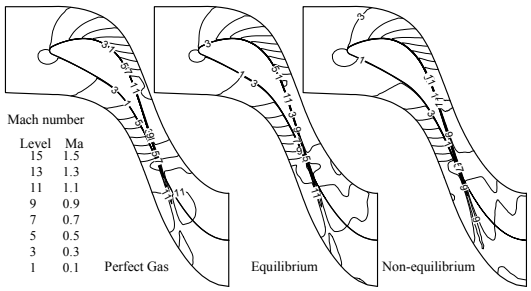

Fig. 5. Mach number distributions at 50% span.

The detail of wetness distributions are shown in Fig. 6. In case 1, there is no wetness exist because the flow medium is just considered as the perfect gas. The results of case 2 and 3 provide the available wetness distributions. In case 2, the results give a much larger wetness than in case 3 especially after the throat of nozzle. That means the flow field given by case 3 is far from the thermodynamic equilibrium state, which is already shown in Fig. 2.

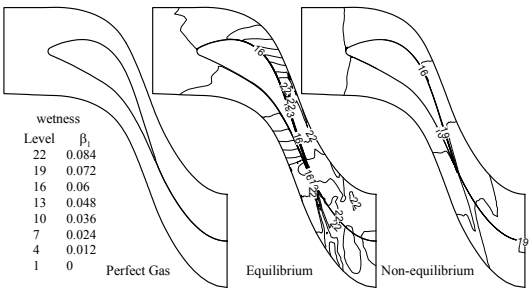

Fig. 6. Wetness distributions at 50% span.

5.2. Comparison of Mass Flow Rate between Numerical Results and Test Data The mass flow rate predicted in three cases is plotted in Fig. 7. The experimental mass flow rate which was measured in a model test steam turbine [9] was provided for the base flow rate of relative mass flow rates.

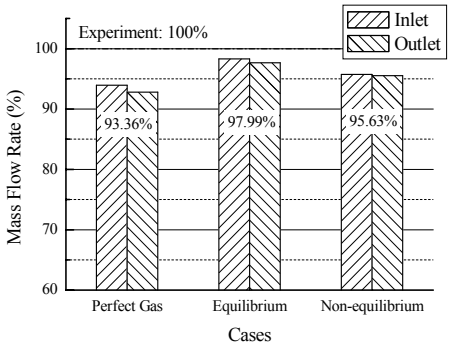

Fig. 7. Comparison of relative mass flow rate between numerical results and test data.

To compare these results, the mass flow rate value predicted in case 2 is closer to the test data than the other two cases. That means the model of equilibrium wet steam is the most appropriate for evaluate the one dimensional mass flow rate of this nozzle blade. It's also obvious that the results of case 3 are more accurate than case 1 but less than case 2. Because the case 3 considers the steam-water phase transformation, its accuracy is better than case 1.

5.3. Comparison of Exit Total Pressure between Numerical Results and Test Data Fig. 8~11 show the exit relative total pressure distributions along pitchwise at 35%, 45%, 55% and 65% span respectively. The relative total pressures are defined as local total pressures divided by inlet average total pressure. They are just similar to the results of mass flow rate, the case 2 gives the best prediction, and the case 3 performs a little better than case 1 but worse than case 2.

6. Conclusions

The higher-order accurate robust CFD method has been extended to the non-equilibrium spontaneous condensing wet steam flow analysis in the last-stage steam turbine nozzle blade. Its dependability has been partly validated by comparing the numerical results with model turbine test data; the equilibrium wet steam model gives the better prediction in the present numerical case. The

classical non-equilibrium spontaneous condensing wet steam flow model needs to be revised more before applying to the complex three dimensional steam-droplet two-phase flows in the steam turbine stage. The present method can be extended to the general real fluid flow analysis easily.

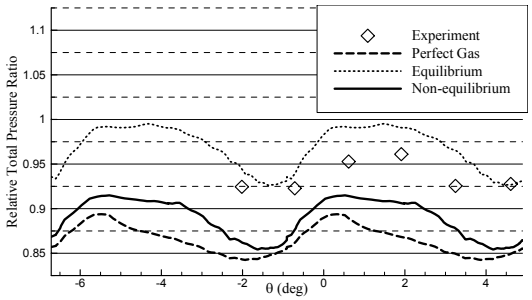

Fig. 8. Exit relative total pressures at 35% span.

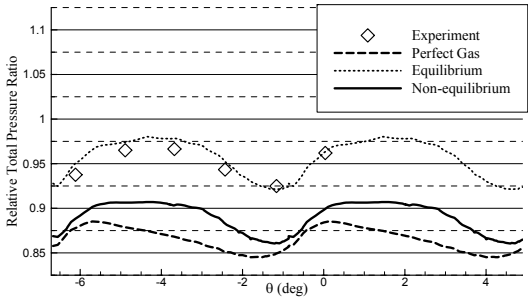

Fig. 9. Exit relative total pressures at 45% span.

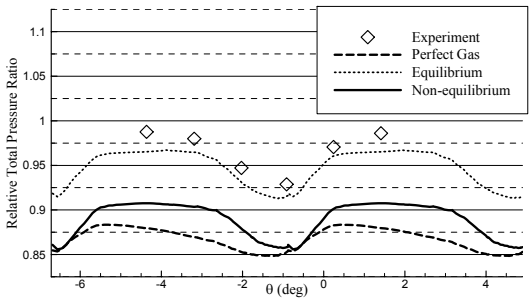

Fig. 10. Exit relative total pressures at 55% span.

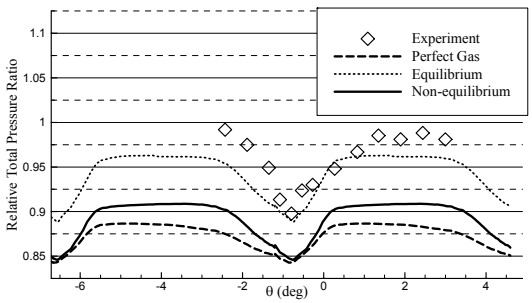

Fig. 11. Exit relative total pressures at 65% span.

Acknowledgements

This work was partially subsidized by the Special Funds for Major State Basic Research Projects (Grant No.G1999022306), and the National Natural Science Foundation of China (Grant No.50076019).

References

[1] J. B. Young, The Spontaneous Condensation of Steam in Supersonic Nozzles, Physicochemical Hydrodynamics, 1982, Vol.3, No.1, pp.57-82.

[2] J. B. Young, The Condensation and Evaporation of Liquid Droplets in a Pure Vapour at Arbitrary Knudsen Number, Int. J. Heat Mass Transfer, 1991, Vol.34, No.7, pp.1649-1661.

[3] K. Ishizaka, T. Ikohagi, and H. Daiguji, A High-Resolution Numerical Method for Transonic Non-Equilibrium Condensation Flows through a Steam Turbine Cascade, Proceedings of 6th International Symposium on Computational Fluid Dynamics, 1995, Vol.I, pp.479-484.

[4] Shigeki Senoo, and Yoshio Shikano, Two-dimensional Analysis for Non-equilibrium Homogeneously Condensing Flows through Steam Turbine Cascade, JSME International Journal, Series B: Fluids and Thermal Engineering, 2002, Vol.45, No.4, pp.865-871.

[5] D. E. Bohn, N. Sürken, and F. Kreitmeier, Nucleation Phenomena in a Multi-Stage Low Pressure Steam Turbine, Journal of Power and Energy, 2003, Vol.217, No.4, pp.453-460.

[6] X. Yuan, and H. Daiguji, A Specially Combined Lower-Upper Factored Implicit Scheme for Three-Dimensional Compressible Navier-Stokes Equations, Computers and Fluids, 2001, Vol.30, No.3, pp.339-363.

[7] H. Daiguji, X. Yuan, and S. Yamamoto, Stabilization of Higher-Order High Resolution Schemes for the Compressible Navier-Stokes Equations, Int. J. of Numerical Methods for Heat & Fluid Flow, 1997, Vol.7, No.2/3, pp.159-182.

[8] X. Yuan, Z. R. Lin, T. Tanuma, et al., Applications of Higher-Order Accurate Computational Fluid Dynamic Method to Steam Turbine Blade Designs, Proceedings of the ICOPE-03, 2003, Kobe, Japan, pp.2-205.

[9] T. Tanuma, S. Nagao, T. Sakamoto, N. Ikeda, M. Matsuda, and K. Imai, The Development of Three-Dimensional Aerodynamic Design Blades for Turbines, JSME Int. J., B, Vol.41, No. 4, (1998).

[10] T. J. Coakley, and P. G. Huang, Turbulence Modeling for High Speed Flows. AIAA Paper 92-0436, 1992.

[11] The Japan Society of Mechanical Engineers, JSME STEAM TABLES, 1999.